IOP Publishing Journal of Physics: Condensed Matter
J. Phys.: Condens. Matter **32** (2020) 125502 (9pp) https://doi.org/10.1088/1361-648X/ab5bdb

Na site doping a pathway for enhanced thermoelectric performance in $Na_{1-x}CoO_2$; the case of Gd and Yb dopants

M Hussein N Assadi

School of Materials Science and Engineering, UNSW Australia, Sydney, NSW 2052, Australia

E-mail: h.assadi.2008@ieee.org

Received 6 October 2019, revised 11 November 2019
Accepted for publication 26 November 2019
Published 24 December 2019

Abstract

Doping is considered to be the main method for improving the thermoelectric performance of layered sodium cobaltate ($Na_{1-x}CoO_2$). However, in the vast majority of past reports, the equilibrium location of the dopant in the $Na_{1-x}CoO_2$' complex layered lattice has not been confidently identified. Consequently, a universal strategy for choosing a suitable dopant for enhancing $Na_{1-x}CoO_2$'s figure of merit is yet to be established. Here, by examining the formation energy of Gd and Yb dopants in $Na_{0.75}CoO_2$ and $Na_{0.50}CoO_2$, we demonstrate that in an oxygen poor environment, Gd and Yb dopants reside in the Na layer while in an oxygen rich environment these dopants replace a Co in CoO_2 layer. When at Na layer, Gd and Yb dopants reduce the carrier concentration via electron–hole recombination, simultaneously increasing the Seebeck coefficient (S) and reducing electric conductivity (σ). Na site doping, however, improves the thermoelectric power factor (PF), only in $Na_{0.50}CoO_2$. When replacing a Co, these dopants reduce S and PF. The results demonstrate how thermoelectric performance critically depends on the synthesis environment that must be fine-tuned for achieving any thermoelectric enhancement.

Keywords:doping, sodium cobaltate, density functional theory, thermoelectric effect

Supplementary material for this article is available online

(Some figures may appear in colour only in the online journal)

Introduction

Sodium cobaltate ($Na_{1-x}CoO_2$) is an interesting compound that exhibits rich magnetic and structural phase diagrams [1–3] and possesses a relatively high thermoelectric figure of merit (ZT) [4] at higher temperatures. As shown in figure 1(a), the $Na_{1-x}CoO_2$ lattice is made of stacked alternating Na layers and edge-sharing CoO_2 octahedra. The mixture of Co^{3+} and Co^{4+} ions in the CoO_2 layer in sodium deficient $Na_{1-x}CoO_2$ generates a Seebeck potential through spin entropy flow [5, 6]. The Seebeck coefficient (S) of polycrystalline $Na_{0.75}CoO_2$ at 800 k is within the range of ~132 μV K^{-1} and ~143 μV K^{-1} depending on the synthesis method [7–9]. This S value is comparable with that of other thermoelectric oxides; For instance, ZnO:Al and $CaMoO_3$:Gd have S values of ~ −110 μV K^{-1} [10] and ~ −225 μV K^{-1} [11] respectively at the same temperature (for comprehensive reviews see [12, 13]). In Na_xCoO_2, phonons, however, are diffusively scattered by the Na^+ ions which are mobile at room temperature [14, 15] reducing the lattice thermal conductivity (κ_L) [16–20] to ~0.01 W cm^{-1} K^{-1} at ~1000 K [21]. This κ_L value is considerably smaller than that of most oxides in which the dominance of covalent bonding causes relatively high κ_L; for instance; ZnO has a κ_L value of ~1.25 W cm^{-1} K^{-1} at ~1000 K [22].

Given the phenomenal and promising low κ_L in $Na_{1-x}CoO_2$, doping has extensively been used to improve the Seebeck coefficient of $Na_{1-x}CoO_2$ further with the ambition of bringing its ZT to values above unity [7, 8, 21, 23–32]. Nonetheless, dopants have usually been chosen based on the mere nominal oxidation state, atomic mass considerations and the solubility

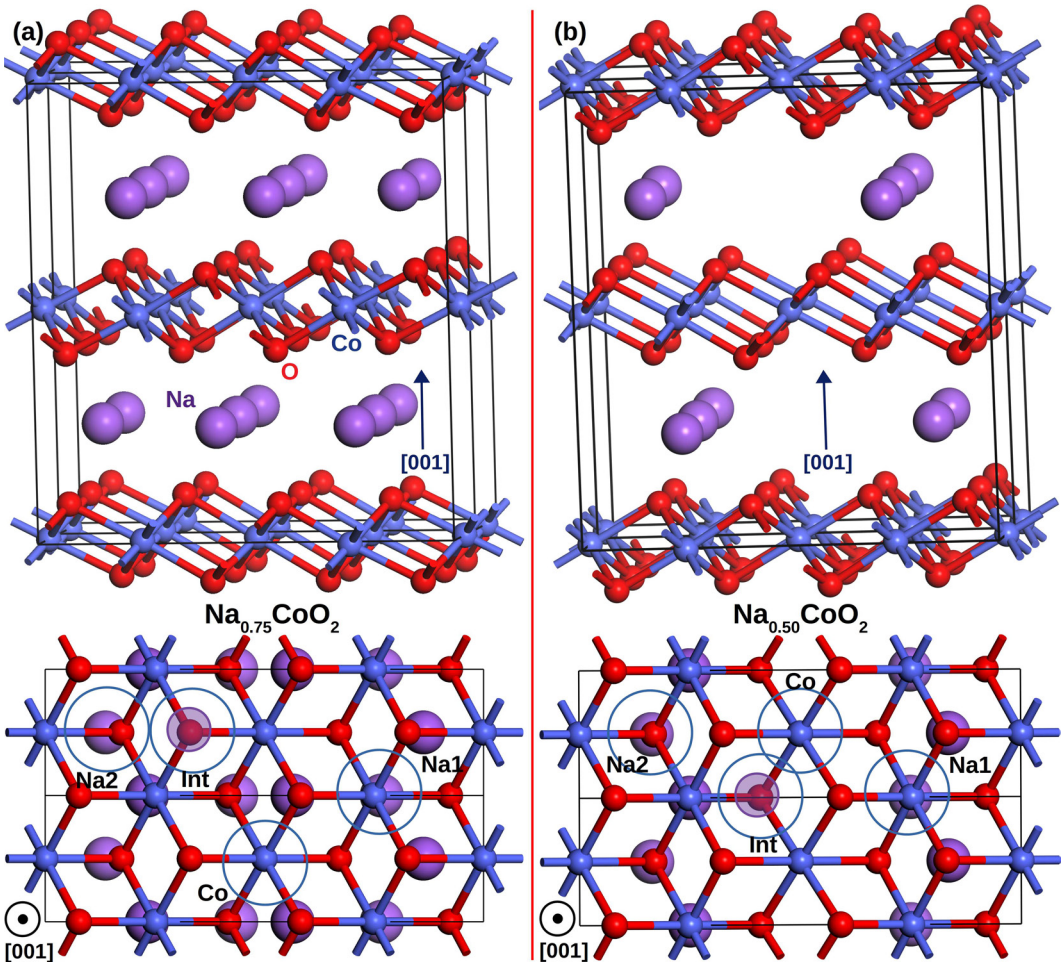

Figure 1. A side (upper panels) and top (lower panels) preview of the $Na_{0.75}CoO_2$ and $Na_{0.50}CoO_2$ supercells is provided in (a) and (b), respectively. Co and O ions occupy the Wyckoff 2*a* and 4*f* sites of the hexagonal lattice structure respectively. In $Na_{0.75}CoO_2$ compound, one-third of the Na ions occupy 2*b* (Na1) sites which share basal coordinates with Co and two-thirds of Na ions occupy 2*c* (Na2) sites which share basal coordinates with O. In $Na_{0.50}CoO_2$ half of the Na ions occupy Na1 site while the other half occupy Na2 sites. The halftone circles represent the location of the interstitial dopants that is vacant in the undoped compounds.

limits of the applied synthesis method [33]. An overlooked issue, nonetheless, is that cationic dopants can be principally substituted for either Na or Co ions. Identifying the exact location of the cationic dopant in $Na_{1-x}CoO_2$'s lattice under a specific condition requires characterisations sensitive to the local chemical environments such as x-ray absorption spectroscopy and neutron diffraction which are most often absent from the existing reports so far. Consequently, despite the large volume of research on doped $Na_{1-x}CoO_2$, the experimental advancement in the doped $Na_{1-x}CoO_2$ has been mainly guided by the approximate guesswork rather comprehensive and strategic insight of how dopants influence the *ZT* through structure-property relationship. As a result, not only the initial ambition of achieving a *ZT* comfortably greater than one has not been realised yet but also many theoretically interesting questions have remained unanswered.

In this work, therefore, we examine the energetics and the electronic structure of Gd and Yb doped $Na_{1-x}CoO_2$ for $x = 0.25$ and 0.5. Based on the formation energy calculations, we demonstrate that the location of Yb and Gd dopants in $Na_{1-x}CoO_2$ critically depends on the synthesis environment, i.e. these dopants reside in different lattice sites depending on the O partial pressure during the synthesis. The insight obtained here complements our previous work that demonstrated that the location of dopants such as Cu and Au also depends on the Na content of $Na_{1-x}CoO_2$ [34]. One of the main conclusions that we draw in this work is that the location of cationic dopants in $Na_{1-x}CoO_2$ needs to be investigated critically and the simplistic assumption based on matching ionic radii in determining dopant location can be misleading at times.

Computational settings

Total energy density functional calculations were performed using the plane-wave and on-the-fly generated ultra-soft pseudopotential [35] approach, as implemented in CASTEP [36–38]. Ceperley and Alder's local density approximation was used for the exchange-correlation term in the Hamiltonian [39]. Energy cut-off was set to 517 eV, and the *k*-point mesh was set to generate a k point separation of 0.05 $Å^{-1}$ for oxides and 0.01 $Å^{-1}$ for metals. The density-mixing scheme was applied for electronic minimisation during which the spin

of all atoms was initiated based on formal values and then allowed to relax. The scalar relativistic treatment based on Koelling–Harmon approximation of Dirac's equation was also applied [40]. LDA+U correction based on a simplified and rotationally invariant approach was applied to Co 3d and Gd/Yb 4f electrons [41]. The default U values of 2.5 eV for Co and 6.0 eV for rare earth dopants were selected for which a full justification is provided in figure S1 of the supplementary information (stacks.iop.org/JPhysCM/23/125502/mmedia). The lattice parameters of a fully optimised primitive unit cell of Na_1CoO_2 was found to be 2.87 Å for a and 10.90 Å for c reasonably matching the experimental values [42]. The difference was only 0.07% for a and −1.49% for c. Then a $2a \times 4a \times 1c$ Na_1CoO_2 supercell was constructed for studying the doped compounds. Four and then eight out of the sixteen original Na ions were removed according to the previously established patterns [43], shown in figure 1, to create a $Na_{12}Co_{16}O_{32}$ and $Na_8Co_{16}O_{32}$ supercells for $Na_{0.75}CoO_2$ and $Na_{0.50}CoO_2$ compounds, respectively. Further details regarding the convergence with respect to the supercell size is provided in table S1 and figure S2 of the supplementary information. The oxidation state of the dopants and the Co ions was estimated from the magnetisation calculated by Mulliken population analysis and examining the partial density of states. One, however, should note that due to partial covalency in Co–O bond, Co ion magnetisation is slightly smaller than what is anticipated from Hund's rule [44]. The accuracy of Mulliken population analysis was cross-examined with Hirshfeld charge analysis for with the results are provided in table S2. It was found that Mulliken population analysis provides a robust description of charge localisation in doped $Na_{1-x}CoO_2$ compounds.

Results and discussion

Dopants' formation energy (E^f) was calculated for four possible replacement configurations. In the first configuration, the dopant M replaced a Co ion creating an M_{Co} configuration. In the second instant, M occupied an interstitial site in the Na layer, creating a M_{Int} configuration. Third, dopant M replaced a Na ion at Na1 site, creating an M_{Na1} configuration. Finally, M replaced a Na ion at Na2 site, creating an M_{Na2} dopant. As demonstrated in figure 1, Na1 shares the basal coordinates with Co while Na2 shares the basal coordinates with O. The formation energy (E^f) was calculated using the standard procedure as described by the following equation [45]:

$$E^f = E^t\left(Na_{1-x}CoO_2 : M\right) + \mu_\alpha - E^t\left(Na_{1-x}CoO_2\right) - \mu_M. \quad (1)$$

Here, $E^t(Na_{1-x}CoO_2{:}M)$ is the total energy of the $Na_{1-x}CoO_2$ supercell containing the dopant M, and $E^t(Na_{1-x}CoO_2)$ is the total energy of the undoped $Na_{1-x}CoO_2$ supercell. μ_α and μ_M are the chemical potentials of the removed and added elements, respectively. The chemical potentials depend on the synthesis environment [46]. To investigate the thermodynamics of dopant solubility in $Na_{1-x}CoO_2$, we first determined the accessible chemical potentials for Na, Co, O and the dopants Gd and Yb. By varying the chemical potentials (μ) by a permissible value of $\Delta\mu$ ($\mu = \mu^0 + \Delta\mu$), we can simulate the effect of varying the oxygen partial pressures and the abundance of constituting elements on the dopants' formation energy and their location in the host lattice. We, therefore, can determine the optimum conditions for Gd and Yb doping that may enhance the thermoelectric performance. The first constraint on the chemical potentials is set by the enthalpy of the $Na_{1-x}CoO_2$:

$$(1-x)\,\Delta\mu_{Na} + \Delta\mu_{Co} + 2\Delta\mu_O = \Delta H^f\left(Na_{1-x}CoO_2\right) \quad (2)$$

in which $\Delta H^f(Na_{1-x}CoO_2)$ is the DFT formation enthalpy of $Na_{1-x}CoO_2$. Furthermore, to avoid precipitation into solid elemental Co, Na, and the release of gaseous O_2, we also require:

$$\mu_{Na}, \mu_{Co}, \mu_O \leqslant 0. \quad (3)$$

The chemical potentials are further constrained by the decomposition of $Na_{1-x}CoO_2$ into competing binary compounds such as Na_2O, CoO_2 and Co_3O_4:

$$\begin{aligned} &2\Delta\mu_{Na} + \Delta\mu_O = \Delta H^f\left(Na_2O\right), \Delta\mu_{Co} + 2\Delta\mu_O \\ &= \Delta H^f\left(CoO_2\right), 3\Delta\mu_{Co} + 4\Delta\mu_O = \Delta H^f\left(Co_3O_4\right). \end{aligned} \quad (4)$$

For Gd and Yb, $\Delta\mu$ was calculated based on

$$2\Delta\mu_{Gd} + 3\Delta\mu_O = \Delta H^f\left(Gd_2O_3\right), \quad (5)$$

$$\Delta\mu_{Yb} + 2\Delta\mu_O = \Delta H^f\left(YbO\right). \quad (6)$$

Here $Ia\bar{3}$ Gd_2O_3 and $Fm\bar{3}m$ YbO are the most stable Yb and Gd oxides. Finally, the chemical potentials were set equal to the elemental energy of a given metal (μ^0) plus the corresponding $\Delta\mu$.

As shown in figure 2, we found that the major limiting phases are Na_2O in Na rich environment and CoO_2 and Co_3O_4 in Co rich environment for both $Na_{0.75}CoO_2$ and $Na_{0.50}CoO_2$. CoO was not a limiting phase. Furthermore, the available range of the chemical potential was relatively limited by the permissible range of $\Delta\mu_{Na}$, resulting in a narrow strip that had a wider range for $\Delta\mu_{Co}$ and $\Delta\mu_O$. Due to the narrow strip of permissible $\Delta\mu$ values, we only present two extremes when discussing the formation energy. These extremes are marked with A for O poor environment and B for O rich environment in figure 2 (justification is provided in figure S3 and table S3 of the supplementary information).

Figure 3 presents the formation energy of the dopants. Under O poor environment, in $Na_{0.50}CoO_2$ and $Na_{0.75}CoO_2$, both Gd and Yb dopants reside in the Na layer. In the case of Gd doped $Na_{0.75}CoO_2$, Gd_{Int} with an E^f of 5.13 eV was the most stable configuration followed by Gd_{Co} with an E^f of 5.51 eV. In the case of Yd doped $Na_{0.75}CoO_2$, Yb_{Na1} with an E^f of 14.03 eV was the most stable configuration followed by Yb_{Na2} with an E^f of 14.42 eV. In the case of Gd doped $Na_{0.50}CoO_2$, the most stable configuration was Gd_{Int} with an E^f of 0.95 eV followed by Gd_{Na2} with an E^f of 2.36 eV while in the case of Yb doped $Na_{0.50}CoO_2$, the most stable configuration was Yb_{Na2} with an E^f of 12.03 eV followed by Yb_{Int} with an E^f of 12.24 eV.

Under O rich environment, the sequence of the stabilisation was, however, different. In both $Na_{0.50}CoO_2$ and $Na_{0.75}CoO_2$ compounds; Gd and Yb dopants replace a Co ion in the host

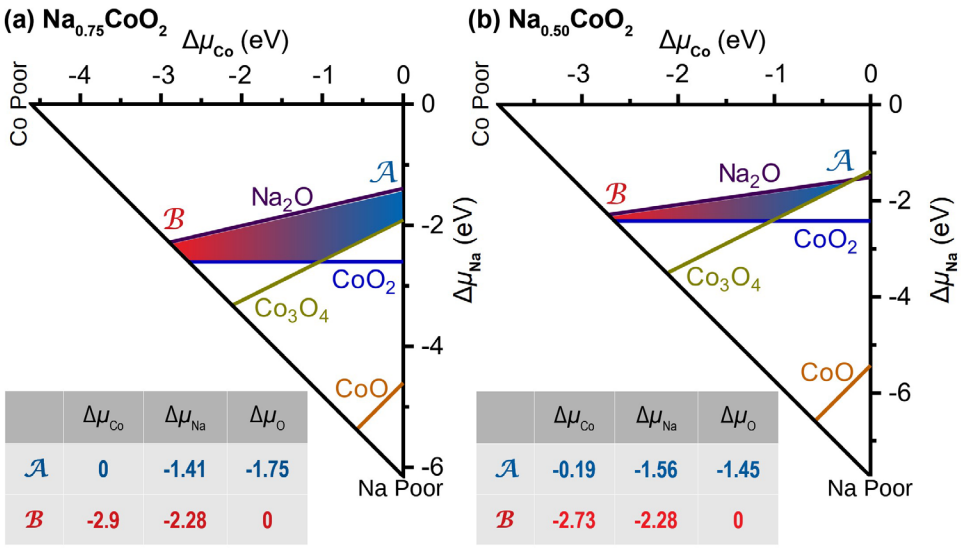

	$\Delta\mu_{Co}$	$\Delta\mu_{Na}$	$\Delta\mu_{O}$
$\mathcal{A}$	0	-1.41	-1.75
$\mathcal{B}$	-2.9	-2.28	0

	$\Delta\mu_{Co}$	$\Delta\mu_{Na}$	$\Delta\mu_{O}$
$\mathcal{A}$	-0.19	-1.56	-1.45
$\mathcal{B}$	-2.73	-2.28	0

Figure 2. The accessible ($\Delta\mu$) chemical potential range. The triangle vertices are determined by the formation enthalpy of (*a*) $Na_{0.75}CoO_2$ and (*b*) $Na_{0.50}CoO_2$, respectively. Limits are imposed by the formation of competing binary phases and result in the shaded stable region. $\Delta\mu$ values are given for points *A* and *B* in eV.

lattice. For Gd doped $Na_{0.75}CoO_2$, Gd_{Co} with an E^f of 4.95 eV had the lowest energy followed by Gd_{Na1} with an E^f of 9.79 eV. For Yd doped $Na_{0.75}CoO_2$, Yb_{Co} with an E^f of 13.32 eV had the lowest energy followed by Yb_{Na1} with an E^f of 14.91 eV. In the case of Gd doped $Na_{0.50}CoO_2$, Gd_{Co} was the most stable configuration with an E^f of 3.08 eV followed by Gd_{Int} with an E^f of 4.31 eV while in the case of Yb doped $Na_{0.50}CoO_2$, the most stable Yb_{Co} configuration had an E^f of 12.69 eV followed by Yb_{Na2} with an E^f of 12.75 eV.

Figure 4 presents the partial density of states (PDOS) of the stable Gd doped configurations in O poor environment, i.e. $Na_{0.75}CoO_2$:Gd_{Int} and $Na_{0.50}CoO_2$:Gd_{Int}, and O rich environment, i.e. $Na_{0.75}CoO_2$:Gd_{Co} and $Na_{0.50}CoO_2$:Gd_{Co}. In all of these configurations, Gd's spin-up channel is completely filled while the spin-down channel is empty indicating that Gd adapts an oxidation state of +3 independent from O partial pressure or Na content. Mulliken population analysis also shows a ~7 $\hbar/2$ magnetisation for Gd in all of these configurations indicating a [Xe] $4f^7 5d^0 6s^0$ electronic configuration, that is Gd^{3+}. For Gd_{Int} which is stable at O poor environment, the three electrons introduced by the interstitial Gd^{3+} reduce three of the Co^{4+} ions in the $Na_{0.75}CoO_2$:Gd_{Int} and $Na_{0.50}CoO_2$:Gd_{Int} to Co^{3+}. As a result, $Na_{0.75}CoO_2$:Gd_{Int} has only one spin bearing Co with a magnetisation of 0.76 $\hbar/2$ (undoped $Na_{0.75}CoO_2$ has a total spin of 3.96 $\hbar/2$ borne on four out of the 16 Co ions in the supercell commensurate with four low-spin Co^{4+} in tetrahedral coordination i.e. $t_{2g}^5 e_g^0$), while $Na_{0.50}CoO_2$:Gd_{Int} has five Co^{4+} ions with a total magnetisation of 4.37 $\hbar/2$. As marked with arrows in figures 4(a) and (c), the introduction of Gd_{Int} has, indeed, reduced the peak height of empty t_{2g} states that indicating a reduction of Co^{4+} concentration. In the case of $Na_{0.75}CoO_2$:Gd_{Co}, the stable configuration at O rich environment, the total spin borne on Co ions was 3.80 $\hbar/2$, very close to the value of the undoped compound, indicating that Gd^{3+} has replaced a Co^{3+} ion leaving the four Co^{4+} ions unaltered. The same argument holds for $Na_{0.5}CoO_2$:Gd_{Co} as the total spin borne on Co ions is 7.2 $\hbar/2$ indicating eight Co^{4+} in the supercell.

The PDOS of Gd doped compounds has some other noticeable features. For instance, as marked with blue bars in figures 4(b) and (d), the filled spin-up Gd 4*f* states of Gd_{Co} spread over the range of $-6\,\text{eV} < E_{Fermi} < -4\,\text{eV}$, while the same states are sharply localised at ~ − 7 eV for Gd_{Int} for both Gd doped $Na_{0.75}CoO_2$ and $Na_{0.50}CoO_2$ compounds. The spread of the Gd_{Co} 4*f* states, although not considered full delocalisation, demonstrate the effect of O coordination and its hybridisation with 4*f* states. Furthermore, the Gd 4*f* and Co^{4+} 3*d* ions have parallel spins in all considered compounds in figure 4 except for $Na_{0.50}CoO_2$:Gd_{Int} for which Gd 4*f* and Co^{4+} 3*d* states are of antiparallel spins.

Figure 5 presents the PDOS of Yb doped compounds that are the most stable at O rich and O poor environments, respectively. For compounds that are most stable at O poor environment, that is Yb_{Na1} in $Na_{0.75}CoO_2$ and Yb_{Na2} in $Na_{0.50}CoO_2$, Yb 4*f* states have a narrow empty peak located just above the Fermi level, marked with arrows in figures 5(a) and (c), indicating that Yb dopant had an oxidation state of +3 i.e [Xe] $4f^{13}6s^0$. Considering the remaining spin borne on Co ions which was 1.96 $\hbar/2$ in $Na_{0.75}CoO_2$:Yb_{Na1} and 5.12 $\hbar/2$ in $Na_{0.50}CoO_2$:Yb_{Na2}, we conclude that Yb^{3+} dopants replacing Na^{1+} introduce two electrons into the compounds reducing two Co^{4+}. Moreover, Co substituting Yb dopants that are stable in O rich environment also adapted +3 oxidation state as demonstrated by the empty 4*f* states marked with arrows in figures 5(b) and (d) and the spin borne on Yb ions of 0.95 $\hbar/2$. In these latter cases, the spin borne on Co ions did not differ much from the values borne in undoped compounds, indicating a Yb^{3+} substituting for a Co^{3+}.

We just demonstrated how the location of both Gd and Yb dopants which critically depend on the O partial pressure, influence the electronic structure of the host material. Now let us examine the implication of dopant's location

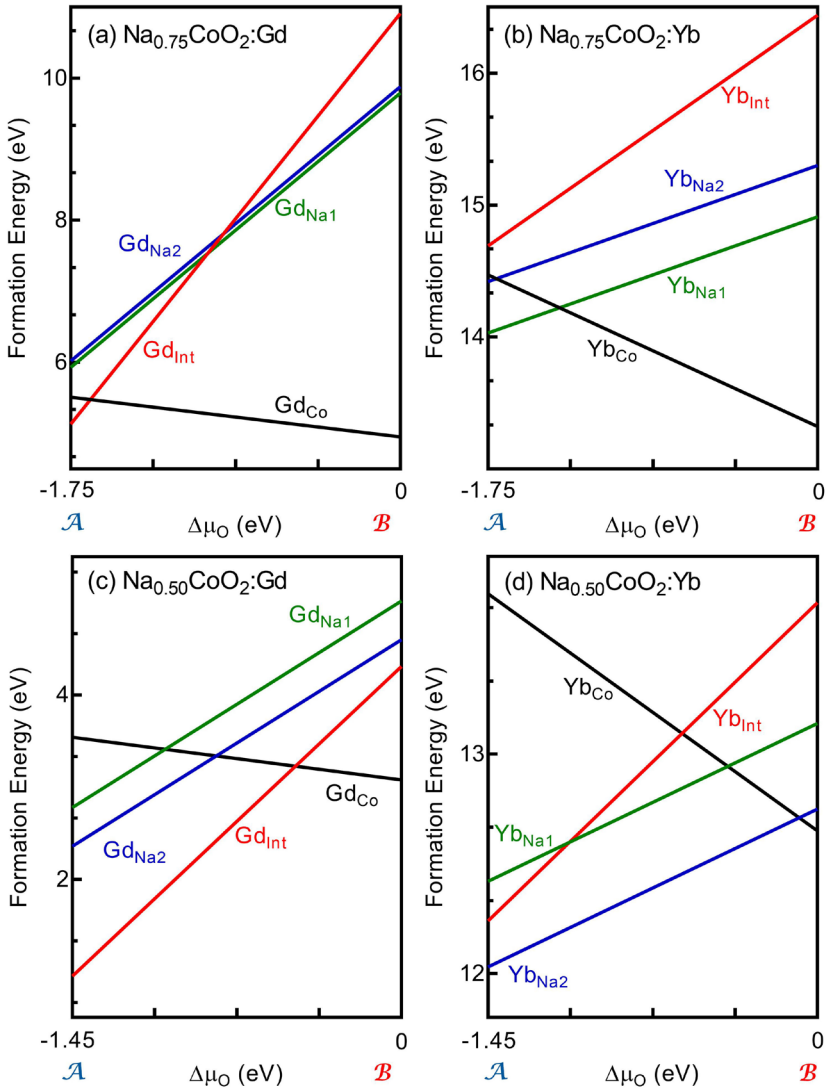

Figure 3. The formation energy of Gd (*a*, *c*), and Yb (*b*, *d*) and Gd dopants in $Na_{0.75}CoO_2$ and $Na_{0.50}CoO_2$ compounds, respectively. Notions *A* and *B* correspond to the points that are marked similarly in figure 2, corresponding to O poor an O rich environments respectively.

on the thermoelectric performance of Gd and Yb doped $Na_{1-x}CoO_2$ in terms of Seebeck coefficient (S), carrier concentration (n), conductivity (σ) and power factor (PF $= S^2\sigma$). The high-temperature Seebeck coefficient in $Na_{1-x}CoO_2$ can be explained by Koshibae's equation [47, 48] for strongly correlated materials which is a modified form of Heikes formula [49, 50]:

$$S\ (T \to \infty) = -\frac{k_B}{e}\ln\left[\frac{g\left(Co^{4+}\right)}{g\left(Co^{3+}\right)}\frac{n_{Co^{4+}}}{n_{Co^{3+}}}\right]. \qquad (7)$$

Here k_B is the Boltzmann constant and e is the electron charge, g equals to the different possible ways in which electrons can be arranged in the orbitals of Co^{3+} and Co^{4+} ions, and n is the concentration of a given species of Co. g can be expressed as the product of spin degeneracy (g_s) and orbital (g_o) degeneracy: $g = g_s \cdot g_o$. g_s equals to $2\zeta + 1$ where ζ is the ions' total spin number while g_o is the number of valid permutations for distributing the electrons across its orbitals. Assuming that Co ions take low spin state in $Na_{1-x}CoO_2$ ($\zeta = 0$ for Co^{3+} and $\zeta = 1/2$ for Co^{4+}), we obtain $g(Co^{4+}) = 6$ and $g(Co^{3+}) = 1$. By substituting these values in the modified Koshibae's formula for S of an electron hopping from a Co^{3+} ion to a Co^{4+} ion, we obtain values of $S = 249\ \mu V\ K^{-1}$ for $Na_{0.75}CoO_2$ and $S = 154\ \mu V\ K^{-1}$ for $Na_{0.50}CoO_2$. It should be noted that Koshibae's formula was obtained by solving the transport problem for a strongly correlated oxide using a Hubbard model at an infinite temperature [51]. The yielded results are, nonetheless, valid for doped $Na_{1-x}CoO_2$, as these compounds are generally intended for waste heat recovery at temperatures higher than ~700 K [12]. For further details see figure S4 of the supplementary information.

Furthermore, we can approximate the conductivity as a function of Co^{4+} concentration by assuming that the carrier mobility remains $1.0\,cm^2\ V^{-1}\ s^{-1}$ for doped $Na_{1-x}CoO_2$ [52] for which full details are provided in table S4. This approximation is somehow conservative as dopants in Na layer are generally expected to improve carrier mobility slightly [34]. This approximation gives a conductivity value of $1.03 \times 10^3\ \Omega^{-1}\ cm^{-1}$ for $Na_{0.75}CoO_2$ and $2.06 \times 10^3\ \Omega^{-1}\ cm^{-1}$ for

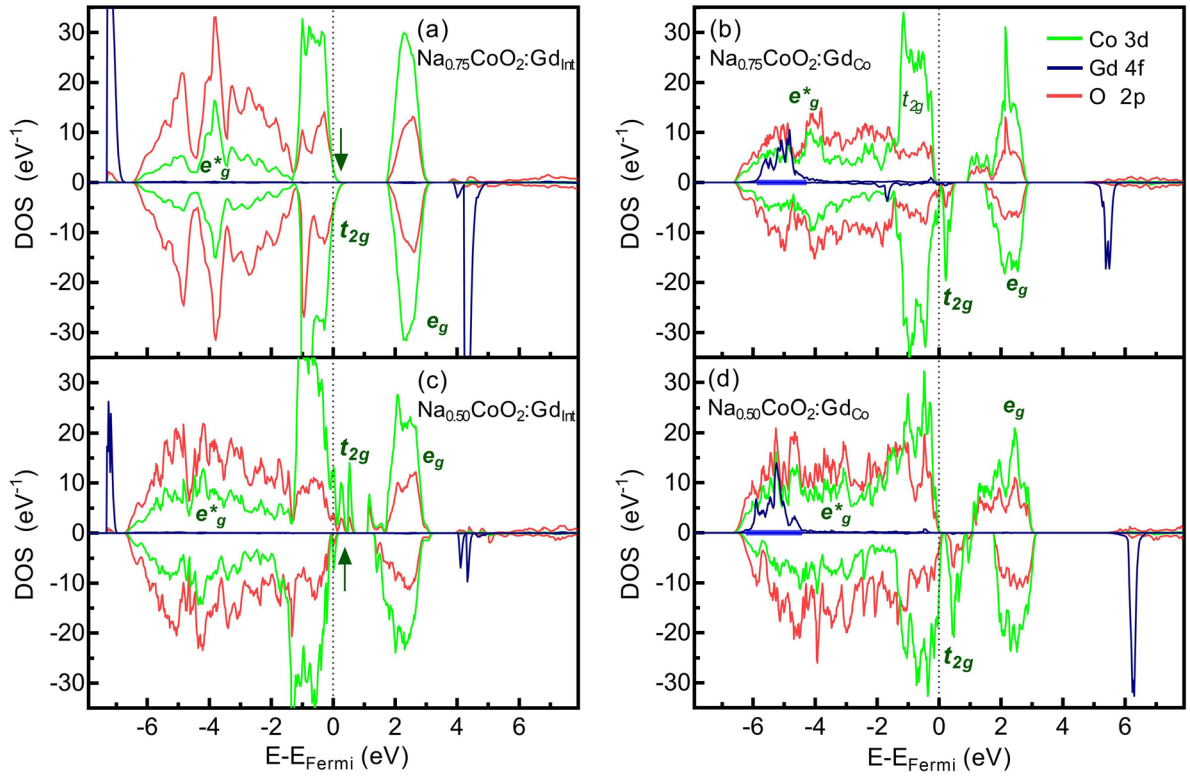

Figure 4. Partial density of states of the most stable doping configurations in O poor environment (left column) and O rich environment (right column) for Gd doped $Na_{0.75}CoO_2$ (top panels) and $Na_{0.50}CoO_2$ (bottom panels). Blue, green and red lines represent Gd 4*f*, Co 3*d* and O 2*p* states, respectively.

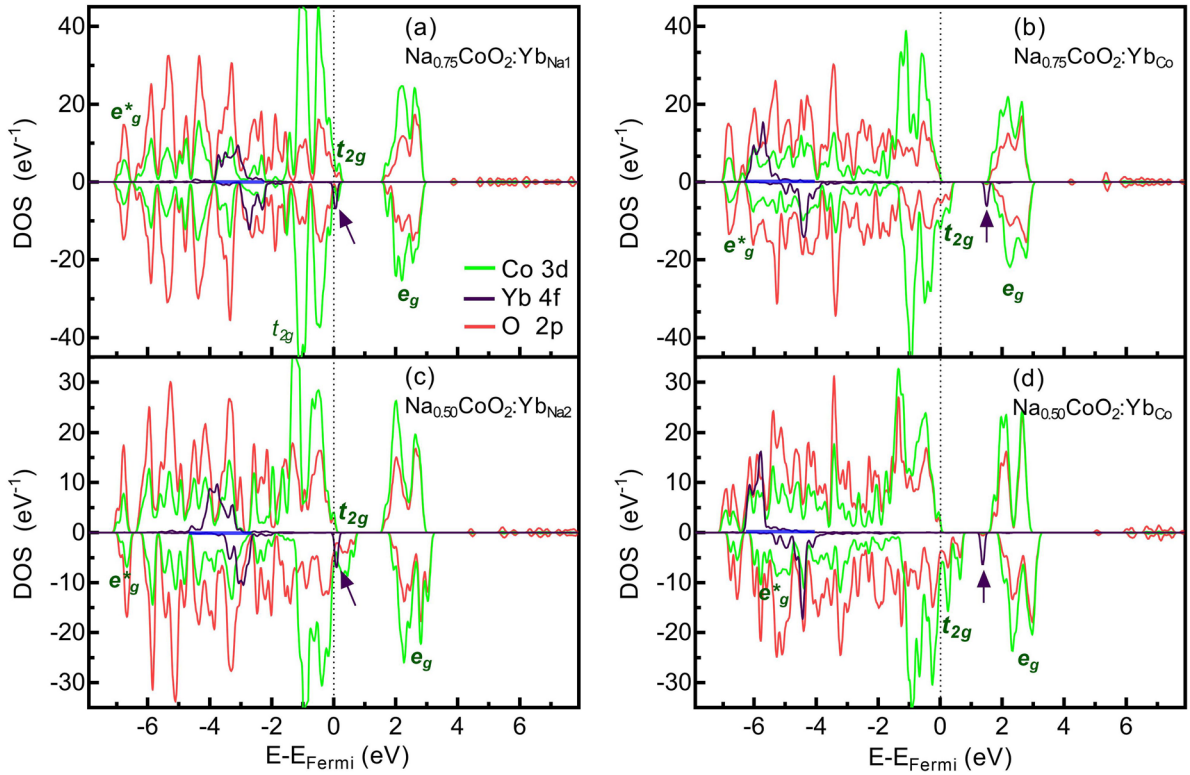

Figure 5. Partial density of states of the most stable doping configurations in O poor environment (left column) and O rich environment (right column) for Yb doped $Na_{0.75}CoO_2$ (top panels) and $Na_{0.50}CoO_2$ (bottom panels). Purple, green and red lines represent Yb 4*f*, Co 3*d* and O 2*p* states, respectively.

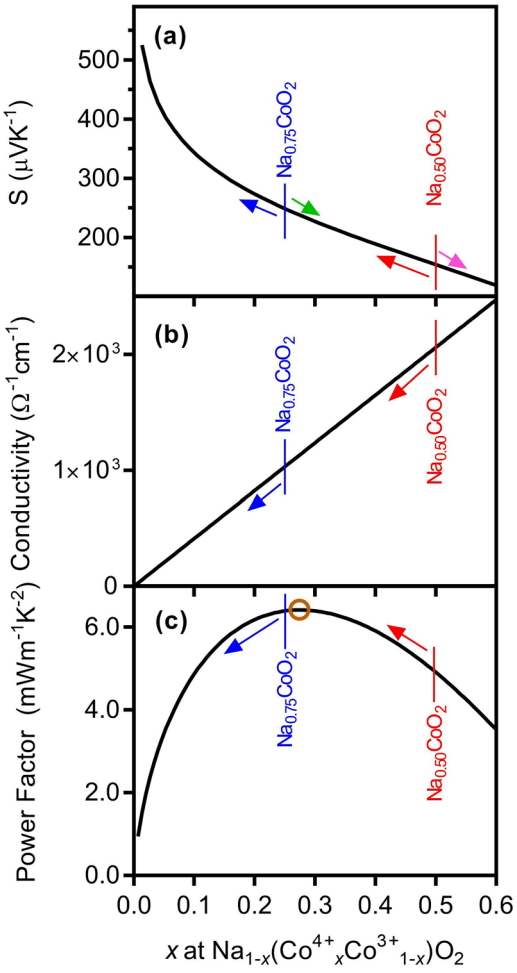

Figure 6. (a) Seebeck coefficient (S) based on Koshibae's equation, (b) conductivity (σ) and (c) the power factor in $Na_{1-x}CoO_2$ as a function of Co^{4+} concentration. Green and pink arrows indicate the change in S for cobalt site doping. The blue and red arrows indicate the change of S, σ and PF for Na site doping.

$Na_{0.50}CoO_2$. The power factor, which is a parabolic function of S and a linear function of σ, comes out as 6.392 mW m^{-1} K^{-2} for $Na_{0.75}CoO_2$ and 4.912 mW m^{-1} K^{-2} in $Na_{0.50}CoO_2$. These values are quite similar to measurements in single-crystal [53, 54] and epitaxial thin film $Na_{1-x}CoO_2$ [55]. The conductivity values, however, are an order of magnitude larger than those measured in polycrystalline samples indicating the significant role of carrier scattering at grain boundaries [56].

In O poor environment, Gd_{Int} is the most stable configuration in both $Na_{0.75}CoO_2$ and $Na_{0.50}CoO_2$. Interstitial Gd^{3+} introduces three electrons that recombine with three holes of the host compound, reducing the concentration of Co^{4+}. As marked with red and blue arrows in figure 6(a), such a reduction in Co^{4+} concentration increases S to 388 μV K^{-1} in $Na_{0.75}CoO_2$:Gd_{Int}, and to 222 μV K^{-1} in $Na_{0.50}CoO_2$:Gd_{Int}. The reduction in Co^{4+} concentration also decreases carrier concentration (n) and conductivity (σ). As marked with red and blue arrows in figure 6(b), Gd_{Int} reduces σ to 2.58 $\times$ 10^2 Ω^{-1} cm^{-1} in $Na_{0.75}CoO_2$:Gd_{Int} and to 1.29 $\times$ 10^3 Ω^{-1} cm^{-1} in $Na_{0.50}CoO_2$:Gd_{Int}. As shown in figure 6(c), the power factor, decreases to 3.873 mW m^{-1} K^{-2} for $Na_{0.75}CoO_2$:Gd_{Int} while it increases to 6.367 mW m^{-1} K^{-2} in $Na_{0.50}CoO_2$:Gd_{Int}. In O poor environment, Yb dopants replace an existing Na. In this case, each Yb dopant introduces two electrons. As a result, the reduction in Co^{4+} concentration and conductivity is less dramatic than the case of Gd doping. For $Na_{0.75}CoO_2$:Yb_{Na1}, S, σ and power factor, therefore, were calculated to be 322 μV K^{-1}, 5.15 $\times$ 10^2 Ω^{-1} cm^{-1} and 5.344 mW m^{-1} K^{-2}, respectively. For $Na_{0.50}CoO_2$:Yb_{Na2}, on the other hand, S, σ and power factor, were calculated to be 198 μV K^{-1}, 1.55 $\times$ 10^3 Ω^{-1} cm^{-1} and 6.085 mW m^{-1} K^{-2} respectively.

Gd^{3+} and Yb^{3+} dopants, when substituting for Co^{3+} as in O rich environment, do not change the carrier (hole) concentration. However, they change the dynamics of spin entropy flow. As shown in figures 4(b), (d), 5(b) and (d), the 4f states of Gd and Yb dopants gravitate towards the bottom of the valence band hybridising with O 2p and Co's bonding e_g^* states. The electric conduction and therfore the spin entropy flow is facilitated by the electrons hopping from a full t_{2g}^6 states of a Co^{3+} ion to a singly vacant t_{2g}^5 states of a Co^{4+} which all are located within ~1 eV of the Fermi level. Consequently, Gd_{Co} and Yb_{Co}, in practice, reduce the Co^{3+} sites available for conduction, increasing the overall concentration of Co^{4+}. Taking the reduced number of Co^{3+} sites into account, as marked with green and pink arrows in figure 6(a), according to Koshibae's equation, S is reduced to 241 μV K^{-1} for $Na_{0.75}CoO_2$ doped with Gd_{Co} and Yd_{Co} and to 142 μV K^{-1} for $Na_{0.50}CoO_2$ doped with Gd_{Co} and Yd_{Co}. The carrier concentration, on the other hand, is not altered by Co side doping as the concentration of hole bearing Co^{4+} does not change by either Gd_{Co} or Yd_{Co} doping. The net result for Co site doping that which is prevalent in O rich environment is, therefore, a net decrease in the power factor.

Earlier experiments have confirmed the possibility of doping in $Na_{0.50}CoO_2$ with Gd and Yb [23, 57]. In the case of Yb doping in $Na_{0.5}CoO_2$, synthesised through solid-state reaction, 5% Yb doping decreased σ by ~25% compared to the undoped compound over the temperature range of 400 – 1000 K (form ~2.94 $\times$ 10^2 Ω^{-1} cm^{-1} to 2.27 $\times$ 10^2 Ω^{-1} cm^{-1}). Yb doping, on the other hand, slightly increased S from ~185 μV K^{-1} to ~205 μV K^{-1} at 800 K [23]. As a result, Yb doping increased the PF to ~1.5 mW m^{-1} K^{-2} from the ~1.2 mW m^{-1} K^{-2} of the undoped sample. The effect of Yb doping on the thermoelectric $Na_{0.50}CoO_2$ is in general agreement with our theoretical prediction. One, however, should note that, as shown in figure 6(c), the PF as a function of carrier concentration has a maximum of 6.416 mW m^{-1} K^{-2} at a Co^{4+} concentration of 0.275. The hypothetical compound $Na_{0.725}CoO_2$ would have the maximum attainable power factor. This composition is, however, above the convex hull of the $Na_{1-x}CoO_2$ phase diagram [58, 59]. As a result, altering Co^{4+} concentration through doping in a stable $Na_{1-x}CoO_2$ composition is the only way to attain the maximum PF value. Consequently, electron doping, such as the case of Yb_{Na} and Gd_{Int}, in the Na layer in $Na_{0.50}CoO_2$ moves the PF towards that maximum while electron doping in $Na_{0.75}CoO_2$ takes the thermopower away from this maximum.

$Ca_3Co_4O_{9\pm\delta}$ is another compound with many similarities to $Na_{1-x}CoO_2$ in which the Seebeck effect originates from the

spin entropy flow from Co^{3+} to Co^{4+} ions. Similar to our prediction for Gd and Yb doping in $Na_{0.50}CoO_2$, Gd doping at 10% in $Ca_3Co_4O_{9+\delta}$ was found to decrease σ from ~100 Ω^{-1} cm^{-1} to ~67 Ω^{-1} cm^{-1} and to increase S from 125 μV K^{-1} to 145 μV K^{-1} at 400 K [60]. Similarly, ~13% Yb doping in $Ca_3Co_4O_{9-\delta}$ was found to decrease σ to ~45 Ω^{-1} cm^{-1} which is half of the value of the undoped compound and to raise S to 155 μV K^{-1} at 400 K [61]. Judging from the combined effect on conductivity and Seebeck coefficient, these dopants, most likely, occupy a Ca site in calcium cobaltate.

Conclusions

Through density functional calculations with LDA + U formalism, we showed that the formation energy of Gd and Yb dopants in $Na_{0.75}CoO_2$ and $Na_{0.50}CoO_2$ was critically sensitive to the synthesis conditions. In an oxygen poor environment, Gd and Yb dopants preferred to occupy a spot in the Na layer while in oxygen rich environment these dopants replaced a Co. Since Gd and Yb have a higher oxidation state than Na, when at Na layer, these dopants reduce the carrier concentration and the electric conductivity via electron–hole recombination and increase the Seebeck coefficient at the same time. The thermoelectric power factor, however, improves only for doped $Na_{0.50}CoO_2$ for which the increased Seebeck coefficient supersedes the reduction in the electric conductivity. When replacing a Co, Gd and Yb dopants reduce the Seebeck coefficient while leaving the electric conductivity unchanged resulting in a net reduction in the power factor.

Acknowledgments

Computational resources were provided by the Integrated Materials Design Centre at UNSW Australia.

ORCID iDs

M Hussein N Assadi https://orcid.org/0000-0002-1559-3211

References

[1] Mendels P, Bono D, Bobroff J, Collin G, Colson D, Blanchard N, Alloul H, Mukhamedshin I, Bert F and Amato A 2005 Cascade of bulk magnetic phase transitions in Na_xCoO_2 as studied by muon spin rotation *Phys. Rev. Lett.* **94** 136403

[2] Berthelot R, Carlier D and Delmas C 2011 Electrochemical investigation of the P2–Na_xCoO_2 phase diagram *Nat. Mater.* **10** 74

[3] Vera E, Alcántar-Vázquez B, Duan Y and Pfeiffer H 2016 Bifunctional application of sodium cobaltate as a catalyst and captor through CO oxidation and subsequent CO_2 chemisorption processes *RSC Adv.* **6** 2162

[4] Fergus J W 2012 Oxide materials for high temperature thermoelectric energy conversion *J. Eur. Ceram. Soc.* **32** 525

[5] Terasaki I, Sasago Y and Uchinokura K 1997 Large thermoelectric power in $NaCo_2O_4$ single crystals *Phys. Rev.* B **56** R12685

[6] Wang Y, Rogado N S, Cava R and Ong N 2003 Spin entropy as the likely source of enhanced thermopower in $Na_xCo_2O_4$ *Nature* **423** 425–8

[7] Tsai P H, Zhang T S, Donelson R, Tan T T and Li S 2011 Power factor enhancement in Zn-doped $Na_{0.8}CoO_2$ *J. Alloys Compd.* **509** 5183

[8] Seetawan T, Amornkitbamrung V, Burinprakhon T, Maensiri S, Kurosaki K, Muta H, Uno M and Yamanaka S 2006 Thermoelectric power and electrical resistivity of Ag-doped $Na_{1.5}Co_2O_4$ *J. Alloys Compd.* **407** 314

[9] Nag A and Shubha V 2014 Oxide thermoelectric materials: a structure-property relationship *J. Electron. Mater.* **43** 962

[10] Zhang D-B, Zhang B-P, Ye D-S, Liu Y-C and Li S 2016 Enhanced Al/Ni co-doping and power factor in textured ZnO thermoelectric ceramics prepared by hydrothermal synthesis and spark plasma sintering *J. Alloys Compd.* **656** 784

[11] Lan J, Lin Y-H, Fang H, Mei A, Nan C-W, Liu Y, Xu S and Peters M 2010 High-temperature thermoelectric behaviors of fine-grained Gd-doped $CaMnO_3$ ceramics *J. Am. Ceram. Soc.* **93** 2121

[12] Feng Y, Jiang X, Ghafari E, Kucukgok B, Zhang C, Ferguson I and Lu N 2018 Metal oxides for thermoelectric power generation and beyond *Adv. Compos. Hybrid Mater.* **1** 114

[13] Liu Y, Wang W, Yang J and Li S 2018 Recent advances of layered thermoelectric materials *Adv. Sustain. Syst.* **2** 1800046

[14] Foo M L, Wang Y, Watauchi S, Zandbergen H, He T, Cava R and Ong N 2004 Charge ordering, commensurability, and metallicity in the phase diagram of the layered Na_xCoO_2 *Phys. Rev. Lett.* **92** 247001

[15] Weller M, Sacchetti A, Ott H, Mattenberger K and Batlogg B 2009 Melting of the Na layers in solid $Na_{0.8}CoO_2$ *Phys. Rev. Lett.* **102** 056401

[16] Mahan G and Sofo J 1996 The best thermoelectric *Proc. Natl Acad. Sci. USA* **93** 7436

[17] Snyder G J and Toberer E S 2008 Complex thermoelectric materials *Nat. Mater.* **7** 105

[18] Voneshen D, Refson K, Borissenko E, Krisch M, Bosak A, Piovano A, Cemal E, Enderle M, Gutmann M and Hoesch M 2013 Suppression of thermal conductivity by rattling modes in thermoelectric sodium cobaltate *Nat. Mater.* **12** 1028

[19] Koumoto K, Terasaki I and Funahashi R 2006 Complex oxide materials for potential thermoelectric applications *MRS Bull.* **31** 206

[20] Roger M *et al* 2007 Patterning of sodium ions and the control of electrons in sodium cobaltate *Nature* **445** 631

[21] Nagira T, Ito M, Katsuyama S, Majima K and Nagai H 2003 Thermoelectric properties of $(Na_{1-y}M_y)$ Co_2O_4 (M = K, Sr, Y, Nd, Sm and Yb; y = 0.01 similar to 0.35) *J. Alloys Compd.* **348** 263

[22] Ozgur U, Gu X, Chevtchenko S, Spradlin J, Cho S J, Morkoc H, Pollak F H, Everitt H O, Nemeth B and Nause J E 2006 Thermal conductivity of bulk ZnO after different thermal treatments *J. Electron. Mater.* **35** 550

[23] Nagira T, Ito M and Hara S 2004 Effect of partial substitutions of rare-earth metals for Na-site on the thermoelectric properties of $Na_xCo_2O_4$ prepared by the polymerized complex method *Mater. Trans.* **45** 1339

[24] Mandal P 2008 Anomalous transport properties of Co-site impurity doped Na_xCoO_2 *J. Appl. Phys.* **104** 063902

[25] Li S, Funahashi R, Matsubara I and Sodeoka S 2000 Magnetic and thermoelectric properties of $NaCo_{2-x}M_xO_4$ (M = Mn, Ru) *Mater. Res. Bull.* **35** 2371

[26] Wang L, Wang M and Zhao D 2009 Thermoelectric properties of c-axis oriented Ni-substituted $NaCoO_2$ thermoelectric oxide by the citric acid complex method *J. Alloys Compd.* **471** 519

[27] Park K, Jang K U, Kwon H C, Kim J G and Cho W S 2006 Influence of partial substitution of Cu for Co on the thermoelectric properties of $NaCo_2O_4$ *J. Alloy. Compd.* **419** 213

[28] Park K and Lee J H 2008 Enhanced thermoelectric properties of $NaCo_2O_4$ by adding ZnO *Mater. Lett.* **62** 2366

[29] Ito M and Furumoto D 2008 Effects of noble metal addition on microstructure and thermoelectric properties of $Na_xCo_2O_4$ *J. Alloys Compd.* **450** 494

[30] Ermawan E and Poertadji S 2015 Thermoelectric properties enhancement of $NaCo_2O_4$ through Ca atom partial substitution on Na atom *Adv. Mater. Res.* **1123** 140

[31] Klyndyuk A I, Krasutskaya N S, Chizhova E A, Evseeva L E and Tanaeva S A 2016 Synthesis and properties of $Na_{0.55}Co_{0.9}M_{0.1}O_2$ (M = Sc, Ti, Cr–Zn, Mo, W, Pb, Bi) solid solutions *Glass Phys. Chem.* **42** 100

[32] Erdal M O, Koyuncu M, Aksu M L, Uslu I and Koçyiğit S 2018 Thermoelectric properties of nickel and boron Co-substituted $NaCo_2O_4$ prepared by electrospinning technique *Nano Hybrid. Compos.* **19** 34

[33] Zhang X and Zhao L-D 2015 Thermoelectric materials: energy conversion between heat and electricity *J. Materiomics* **1** 92

[34] Assadi M H N and Katayama-Yoshida H 2015 Restoration of long range order of Na ions in Na_xCoO_2 at high temperatures by sodium site doping *Comput. Mater. Sci.* **109** 308

[35] Lejaeghere K, Van Speybroeck V, Van Oost G and Cottenier S 2014 Error estimates for solid-state density-functional theory predictions: an overview by means of the ground-state elemental crystals *Crit. Rev. Solid State Mater. Sci.* **39** 1

[36] Clark S J, Segall M D, Pickard C J, Hasnip P J, Probert M I, Refson K and Payne M C 2005 First principles methods using CASTEP *Z. Kristallogr. Cryst. Mater.* **220** 567

[37] Pfrommer B G, Côté M, Louie S G and Cohen M L 1997 Relaxation of crystals with the quasi-Newton method *J. Comput. Phys.* **131** 233

[38] Payne M C, Teter M P, Allan D C, Arias T and Joannopoulos A J 1992 Iterative minimization techniques for *ab initio* total-energy calculations: molecular dynamics and conjugate gradients *Rev. Mod. Phys.* **64** 1045

[39] Ceperley D M and Alder B J 1980 Ground state of the electron gas by a stochastic method *Phys. Rev. Lett.* **45** 566

[40] Koelling D D and Harmon B N 1977 A technique for relativistic spin-polarised calculations *J. Phys. C: Solid State Phys.* **10** 3107

[41] Dudarev S, Botton G, Savrasov S, Humphreys C and Sutton A 1998 Electron-energy-loss spectra and the structural stability of nickel oxide: an LSDA+U study *Phys. Rev.* B **57** 1505

[42] Chen D, Chen H, Maljuk A, Kulakov A, Zhang H, Lemmens P and Lin C 2004 Single-crystal growth and investigation of Na_xCoO_2 and $N_xCoO_2 \cdot yH_2O$ *Phys. Rev.* B **70** 024506

[43] Assadi M H N and Katayama-Yoshida H 2015 Interplay between magnetism and Na concentration in Na_xCoO_2 *Funct. Mater. Lett.* **08** 1540016

[44] Assadi M H N and Katayama-Yoshida H 2019 Covalency a pathway for achieving high magnetisation in $TMFe_2O_4$ compounds *J. Phys. Soc. Japan* **88** 044706

[45] Freysoldt C, Grabowski B, Hickel T, Neugebauer J, Kresse G, Janotti A and Van de Walle C G 2014 First-principles calculations for point defects in solids *Rev. Mod. Phys.* **86** 253

[46] Reuter K and Scheffler M 2001 Composition, structure, and stability of RuO_2 (1 1 0) as a function of oxygen pressure *Phys. Rev.* B **65** 035406

[47] Terasaki I 2011 High-temperature oxide thermoelectrics *J. Appl. Phys.* **110** 053705

[48] Koshibae W, Tsutsui K and Maekawa S 2000 Thermopower in cobalt oxides *Phys. Rev.* B **62** 6869

[49] Heikes R R and Ure R W 1961 *Thermoelectricity: Science and Engineering* (New York: Interscience)

[50] Chaikin P M and Beni G 1976 Thermopower in the correlated hopping regime *Phys. Rev.* B **13** 647

[51] Mukerjee S 2005 Thermopower of the Hubbard model: effects of multiple orbitals and magnetic fields in the atomic limit *Phys. Rev.* B **72** 195109

[52] Brinks P, Rijnders G and Huijben M 2014 Size effects on thermoelectric behavior of ultrathin Na_xCoO_2 films *Appl. Phys. Lett.* **105** 193902

[53] Fujita K, Mochida T and Nakamura K 2001 High-temperature thermoelectric properties of $Na_xCoO_{2-\delta}$ single crystals *Japan. J. Appl. Phys.* **40** 4644

[54] Thinaharan C, Aswal D K, Singh A, Bhattacharya S, Joshi N, Gupta S K and Yakhmi J V 2004 Growth and morphology of the single crystals of thermoelectric oxide material Na_xCoO_2 *Cryst. Res. Technol.* **39** 572

[55] Yu L, Gu L, Wang Y, Zhang P X and Habermeier H U 2011 Epitaxial layered cobaltite Na_xCoO_2 thin films grown on planar and vicinal cut substrates *J. Cryst. Growth* **328** 34

[56] Tellier C R 1978 A theoretical description of grain boundary electron scattering by an effective mean free path *Thin Solid Films* **51** 311

[57] Gunawan B K 2007 The development of rare earth doped $NaCo_2O_4$ thermoelectric materials, *Master's thesis, School of Materials Science and Engineering* (The University of New South Wales, Sydney, Australia)

[58] Meng Y S, Hinuma Y and Ceder G 2008 An investigation of the sodium patterning in Na_xCoO_2 ($0.5 < x < 1$) by density functional theory methods *J. Chem. Phys.* **128** 104708

[59] Zhang P, Capaz R B, Cohen M L and Louie S G 2005 Theory of sodium ordering in Na_xCoO_2 *Phys. Rev.* B **71** 153102

[60] Liu H Q, Zhao X B, Liu F, Song Y, Sun Q, Zhu T J and Wang F P 2008 Effect of Gd-doping on thermoelectric properties of $Ca_3Co_4O_{9+\delta}$ ceramics *J. Mater. Sci.* **43** 6933

[61] Xu J, Wei C and Jia K 2010 Thermoelectric performance of textured $Ca_{3-x}Yb_xCo_4O_{9-\delta}$ ceramics *J. Alloys Compd.* **500** 227